This article has been accepted for publication in a future issue of this journal, but has not been fully edited. Content may change prior to final publication.
Citation information: DOI: 10.1109/TCCN.2025.3586219, IEEE Transactions on Cognitive Communications and Networking

Ambient IoT: Backscatter-based Connectivity Topologies and Outage Behavior

Azzam Al-nahari, Riku Jäntti, *Senior Member, IEEE*, Deepak Mishra, *Senior Member, IEEE*, and Yi Zhou, *Member, IEEE*

***Abstract*—Advancements in low-power and cost-effective backscatter communications are enhancing connectivity for battery-constrained devices, as highlighted by 3GPP's recent ambient Internet-of-things (A-IoT) study. This paper presents a comprehensive analysis of the outage behavior exhibited by various A-IoT backscatter communication topologies, including direct connection with the base station (Topology 1), relay-assisted backscattering (Topology 2), and user equipment-assisted backscattering (Topology 3). For each topology, the outage event is characterized and the outage probability expression is derived. Additionally, asymptotic analysis is performed to study the outage behavior of each topology at high transmit SNR γ_o. The results show that at high SNR, the outage probability scales as $(1/\sqrt{\gamma_o})$ for Topology 1 with symmetric channel, $(1/\gamma_o^{3/2})$ for Topology 2, and $(1/\gamma_o)$ for Topology 3 and Topology 1 with frequency division duplex (FDD) transmission. Through analytical modeling and extensive simulations, our study provides insights into the outage behaviors of these topologies. It is found that the distance of the backscatter link significantly affects outage performance across these topologies. Specifically, Topology 2 shows superior performance at shorter distances, while Topology 3 is more effective at longer distances. Moreover, the impact of backscatter coefficient and target transmission rate on performance is investigated.**

***Index Terms*—Ambient IoT, backscatter communications, symbiotic radio, DF relaying, outage probability.**

I. Introduction

A. Background and Motivation

The Internet of things (IoT) is expected to revolutionize how we interact with technology and the world around us [1], with applications ranging from smart homes and fitness trackers to industrial sensors and agricultural monitors [2]. However, energy efficiency and spectrum scarcity remain key challenges for large-scale IoT deployment. By achieving ultra-low power consumption and employing cognitive spectrum efficiency techniques, IoT devices can operate effectively in various environments, ensuring continuous data collection, analysis, communication, and sustainable performance. The main contemporary machine-type communications (MTC) standards include licensed narrowband IoT (NB-IoT), long-term evolution MTC (LTE-M) [3], and reduced capability (RedCap) new radio [4]. These systems enable simpler, energy-efficient, and cost-effective radio modems that are utilized in mobile broadband applications. However, for several low-end IoT applications, the battery life and device cost of contemporary MTC solutions are still too restrictive.

In a recent development, the 3rd Generation Partnership Project (3GPP) has launched study items focused on the concept of ambient IoT (A-IoT) [5], [6]. The objective is to address the aforementioned limitations and provide low-cost, battery-free connectivity for IoT devices [7], [8]. The term 'ambient' refers to the surrounding environment, indicating the potential for A-IoT devices to harvest energy from ambient sources and be extensively deployed in close proximity to users, enabling comprehensive environmental monitoring in residential and commercial spaces. Backscatter communication techniques [9]–[12] are considered the primary enabling technology for A-IoT. When integrated with existing mobile communication systems, A-IoT is expected to represent the next evolutionary step in MTC. Although existing research has explored A-IoT devices and their potential applications [8], [13], there remains a lack of comprehensive studies on integrating these technologies with various connectivity topologies and evaluating their performance. This gap motivates the present study, which examines the integration of A-IoT devices into existing infrastructure using different communication topologies, and assesses their performance using outage probability—a metric particularly suited to the variable and intermittent signal strength characteristic of low-power, low-cost devices.

B. State of the Art

This subsection outlines the primary backscatter communication configurations pertinent to this paper and reviews their relevant outage performance as reported in the literature.

1) Monostatic Backscattering: Monostatic backscattering involves a reader with a full-duplex receiver, enabling it to both generate the unmodulated carrier signal and receive the backscattered signal from the backscatter device. It is widely utilized in radio frequency identification (RFID) systems [14]. However, full-duplex operation introduces complexity and increases costs, while the presence of round-trip path loss degrades performance. The performance of monostatic backscattering has been extensively studied in the literature [11], [15], [16], [17], and references therein.

The work of A. Al-nahari and R. Jäntti was supported in part by the European Project Hexa-X II under (grant 101095759) and Business Finland Project eMTC (Dnro 8028/31/2022). The work of D. Mishra was partly supported by the Australian Research Council's Discovery Early Career Researcher Award (DECRA) - DE230101391. The work of Y. Zhou is supported by UKRI Postdoc Guarantee project S-ISAC [grant number EP/Z002435/1] and EU MSCA Postdoctoral Fellowships [grant number 101154926].

A. Al-nahari is with the Department of Information and Communications Engineering, Aalto University, 02150 Espoo, Finland, and also with Department of Electrical Engineering, Ibb University, Ibb, Yemen (e-mail: azzam.al-nahari@aalto.fi).

R. Jäntti is with the Department of Information and Communications Engineering, Aalto University, 02150 Espoo, Finland (e-mail: riku.jantti@aalto.fi).

D. Mishra is with the School of Electrical Engineering and Telecommunications, University of New South Wales (UNSW), Sydney, NSW 2052, Australia (e-mail-d.mishra@unsw.edu.au).

Y. Zhou is with the Key Lab of Information Coding, and Transmission, Southwest Jiaotong University, Chengdu 610031, China, and also with Brunel University London, London, UB8 3PH, UK (e-mail: yizhou@swjtu.edu.cn).

This article has been accepted for publication in a future issue of this journal, but has not been fully edited. Content may change prior to final publication.
Citation information: DOI: 10.1109/TCCN.2025.3586219, IEEE Transactions on Cognitive Communications and Networking

2) Bistatic Backscattering: In this configuration, the emitter and reader are geographically separated into two distinct entities [18]. This model can help achieve a longer range and avoid the self-interference, though it comes at the expense of increased costs due to the need for deploying dedicated radio frequency (RF) sources.

3) Ambient Backscattering: In this extensively studied model, an uncontrollable ambient RF source acts as the emitter, while a dedicated reader decodes the information backscattered from the tags [19]. A primary challenge associated with this model is the direct link interference at the reader. Numerous studies have investigated the outage behavior of ambient backscatter communication [20], [21], [22]. In [20] and [21], the authors analyzed the outage performance of ambient backscatter systems, considering the primary link as interference at the backscatter receiver. In [22], the outage performance of multiple backscatter devices was examined, where the reflection coefficient was optimized to improve performance. It is worth noting that the works in [20]–[22] assumed that the primary and secondary backscatter systems operate independently without collaboration.

4) Symbiotic Radio: A significant variant of ambient backscatter communication, known as symbiotic radio (SR) [23], [24], [25], [26] aims to design receivers capable of concurrently capturing both the ambient signal and the backscattered signal, thereby enhancing reliability and spectral efficiency. To achieve this, a successive interference cancellation (SIC) receiver can be employed to effectively decode both signals. Considering a cooperative receiver for decoding both the primary and backscattered signals, the authors in [27] investigated the outage performance of three SR paradigms proposed in [28]. The outage probabilities were analyzed based on optimizing the transmit power and reflection coefficient of the backscatter device. In [29], closed-form expressions for the outage probability of an SR system with two backscatter devices were derived. In [30], the outage performance and ergodic capacity of different SR configurations were studied, with the coexistence outage probability (COP) introduced as a performance metric for the considered SR cases.

5) Relay-assisted Backscattering: A related configuration discussed in the literature involves the use of relays in backscatter communications. The work in [31] proposed a relay-assisted ambient backscattering system, in which a decode-and-forward (DF) relay node simultaneously assists the transmission of both the primary system and the backscatter system. The outage probability and throughput of both relaying links were derived. More recently, the work in [32] analyzed the outage performance of a relay-assisted cooperative ambient backscatter network, where a relay node forwards both the long packets from the primary transmitter and the short packets from the backscatter transmitter. Additionally, the outage performance of a dual-hop DF cooperative ambient backscatter system with single-relay selection was studied in [33].

C. Contribution and Organization

Inspired by the 3GPP's exploration into radio access network (RAN) plenary [6] regarding deployment topologies for A-IoT, we consider three main topologies as shown in Fig. 1.

1) Topology 1 (T1): In this topology, the A-IoT device directly and bidirectionally communicates with a BS-type node. This corresponds to monostatic backscatter communications, where the reader, i.e., BS, utilizes a full-duplex transceiver. One variation is to consider symmetric forward and backward channels, **T1(a)**; this topology and its outage performance are well-established in RFID and monostatic backscattering literature and are included in this discussion for benchmark comparison. Additionally, we consider another case in which the forward and backward channels are uncorrelated, **T1(b)**. This scenario is motivated by the ability of the A-IoT device to shift the frequency of the backscattered signal to a different band, as demonstrated in [34], [35]. This topology could be utilized in frequency division duplex (FDD) transmission without requiring changes to the BS hardware.

2) Topology 2 (T2): In this topology, the A-IoT device is connected to the BS through a relay. We consider the DF protocol at the relay, where the transmission is divided into two phases. In the first phase, the relay transmits a carrier signal that illuminates the A-IoT device, and the resulting backscattered information signal is received by both the relay and the BS. In the second phase, the relay transmits the decoded signal to the BS, provided it was successfully decoded during the first phase. Given that the user equipment (UE) can act as a relay node, T2 is particularly suitable for indoor-to-outdoor communication scenarios for A-IoT [6]. It is important to note that the operational principles of the relay node, as proposed in [31], [32], and [33], differ from the T2 framework utilized in this study. In [31] and [32], the relay acts as a receiver for the SR system, decoding both the primary and backscatter signals before forwarding them to the receiver. In contrast, in T2, the relay first collects the information from the A-IoT device in the first phase and then forwards the signal to the BS in the second phase. Furthermore, the work in [33] studied the impact of relay selection on the outage performance, where the selected relay node acts as a source for SR system, and the relay does not process the signal of the A-IoT device. Thus, studying the performance of T2 in its current form is novel.

3) Topology 3 (T3): In this topology, we consider two scenarios where the UE assists the A-IoT device: UE-assisted uplink data transmission, **T3(a)**, and UE-assisted downlink data transmission, **T3(b)**. In T3(a), the UE transmits an uplink signal to the BS, which also serves as an illuminating signal for the A-IoT device. T3(a) corresponds to SR communication, wherein the A-IoT device transmits its signal by piggybacking on the UE signal. A cooperative receiver at the BS is used to demodulate the two signals using the SIC technique. In contrast, in T3(b), the BS transmits a downlink signal to the UE, which simultaneously illuminates the A-IoT device. The UE then jointly decodes the downlink data and the A-IoT message. To facilitate this task, known signals, such as LTE cell-specific reference signals (LTE-CRS), could be utilized. Recently, the work in [35] proposed a system that uses LTE-CRS transmitted by the BS as an ambient source and experimentally validated the UE-assisted A-IoT on LTE downlink. After decoding the backscattered signal, the UE sends it back to the BS through the backhaul link.

The outage performance metrics for T3(a) and T3(b) considered in this paper differ from those proposed in [27],

This article has been accepted for publication in a future issue of this journal, but has not been fully edited. Content may change prior to final publication.
Citation information: DOI: 10.1109/TCCN.2025.3586219, IEEE Transactions on Cognitive Communications and Networking

[29], [30]. In [27] and [29], the outage probability of the SR system was derived with a simplified channel model, where the cascaded backscatter link consists of a single Rayleigh channel, resulting in outage expressions that are simplified and distinct from those in the current study. Moreover, in [27], although SIC is applied at the backscatter receiver to mitigate the primary signal, it is noteworthy that the primary receiver is distinct from the backscatter receiver. The study in [30] introduced the COP performance metric for SR systems, defining a coexistence outage event where either the primary or the backscatter transmission fails. However, this metric may not fully capture scenarios where, following the SIC principle, the primary system can successfully decode its signal even if the backscatter system is in outage, due to the standard practice of decoding the primary signal first. In contrast, in the proposed T3(a) and T3(b), we assess the outage performance of the primary and backscatter systems separately and compare them, as will be elaborated upon in Section IV-A. In addition, the asymptotic outage performance and diversity order of both topologies are derived.

Our main contributions are summarized as follows

- We introduce a comprehensive framework that explores various backscatter-based connectivity topologies for A-IoT, including direct connectivity with the BS (T1), relay-assisted backscattering (T2), and UE-assisted backscattering (T3). Our objective is to assess and compare the performance of these topologies, with a particular focus on outage behavior. While not exhaustive, these topologies represent fundamental configurations recommended by 3GPP [6].
- We derive closed-form expressions for the outage probability across various topologies, analyzing their performance under different conditions. The results reveal nontrivial performance comparisons among the topologies with varying system parameters. For instance, while relay-assisted backscattering achieves better diversity order at high SNR, it does not consistently outperform other topologies, especially under low SNR conditions and high target transmission rates.
- We conduct an asymptotic analysis of the outage probability in the high SNR γ_o regime. The scaling behavior and diversity order of the different topologies at high SNR are investigated. It is shown that at high SNR, the outage probability scales as $(1/\sqrt{\gamma_o})$ for T1(a) , as $(1/\gamma_o^{3/2})$ for T2, and as $(1/\gamma_o)$ for T1(b), T3(a), and T3(b).
- Numerical results are presented to fairly compare the topologies in terms of deployment distances and total power budget, while also examining the impact of key system parameters on outage performance.

The remainder of this paper is organized as follows. In Section II, the system and channel models are introduced. In Section III, the outage probability of the different connectivity topologies is derived. The asymptotic analysis and diversity order are also discussed. Section IV presents the numerical results, along with discussions on practical aspects and future research directions. Section V provides the concluding remarks.

We use $\mathcal{CN}(\mu, \sigma^2)$ to denote the complex Gaussian random variable with mean μ and variance σ^2. The cumulative distribution function (CDF) and probability density function (PDF) are represented as $F_X(.)$ and $f_X(.)$, respectively. $X \sim \exp(\beta)$ denotes an exponentially distributed random variable with parameter β, where $f_X(x) = \beta e^{-\beta x}$.

II. System Model

We consider an A-IoT backscatter communication environment with different topologies, as shown in Fig. 1. The system consists of a BS, an A-IoT device, a Relay, and a UE. It is assumed that all nodes are equipped with a single antenna and that all channels follow Rayleigh fading[1]. The A-IoT device utilizes backscatter modulation to transmit information to the BS, which may be deployed as a macro, micro, or pico cell. The BS functions as the central node for collecting A-IoT data. We denote the channel gain between nodes i and j in topology τ as $h_{ij}^{\tau} \sim \mathcal{CN}(0, \beta_{ij}^{\tau})$, where $i, j \in \{b = \text{BS}, a = \text{AIoT device}, r = \text{relay}, u = \text{UE}\}$, and $\tau \in \{\text{T1(a)}, \text{T1(b)}, \text{T2}, \text{T3(a)}, \text{T3(b)}\}$. For notational convenience in the following analysis, we omit the factor τ, and the relevant value is implicitly understood from the context of the section.

A. Topology 1 (T1): Direct Connectivity with the BS

In this topology, the BS functions as the reader in a monostatic backscatter communication system. A full-duplex transceiver at the BS is assumed[2]. The BS emits a carrier signal s, where $\mathbb{E}[|s^2|] = 1$, while simultaneously receiving the backscattered signal from the A-IoT device. The received signal at the BS is thus given by

$$y_b = \sqrt{\alpha P} h_{ab} h_{ba} s c + n_b, \tag{1}$$

where P denotes the transmit power, c represents the information signal backscattered from the A-IoT device, with $\mathbb{E}[|c^2|] = 1$, $n_b \sim \mathcal{CN}(0, \sigma_o^2)$ is the additive white Gaussian noise (AWGN), and α is the reflection coefficient at the A-IoT device. We will consider two cases: full-duplex receiver with channel reciprocity, and FDD transmission.

1) T1(a): Full-Duplex Receiver with Channel Reciprocity: In this case, due to channel reciprocity, the forward and backward channels h_{ba} and h_{ab} are fully correlated, implying $h_{ba} = h_{ab}$. Moreover, as mentioned earlier, the BS is assumed to filter out the self-interference carrier signal. Thus, the instantaneous SNR of at the BS is

$$\gamma_b^{\text{T1(a)}} = \frac{\alpha P \left| h_{ba} \right|^4}{\sigma_o^2}. \tag{2}$$

[1]In this paper, our objective is to evaluate the performance and diversity order of the various topologies and compare them, rather than focusing on the performance achieved by MIMO diversity gain. Consequently, we assume a single antenna at the BS. Additionally, as demonstrated in [34] and [35], a single antenna is also assumed and utilized at the BS for UE-assisted ambient backscattering in the LTE downlink.

[2]Note that as the BS transmits an unmodulated single carrier signal, the receiver can easily decouple its own self-jamming carrier, which is a commonplace in the literature [11], [36], [37], and is considered in our work.

This article has been accepted for publication in a future issue of this journal, but has not been fully edited. Content may change prior to final publication. Citation information: DOI: 10.1109/TCCN.2025.3586219, IEEE Transactions on Cognitive Communications and Networking

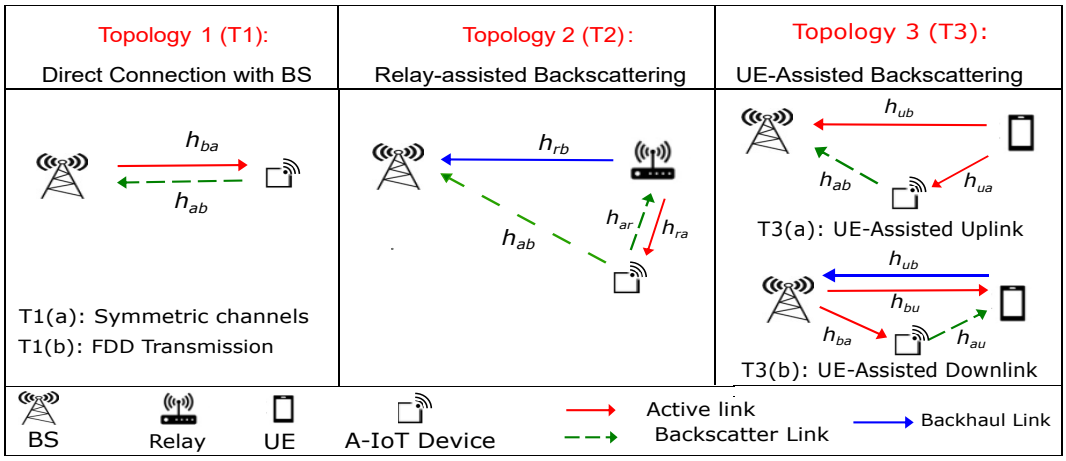

Fig. 1. Illustration of the different A-IoT topologies. **Topology 1 (T1)**: The A-IoT device is in direct connectivity with the BS. **Topology 2 (T2)**: Relay-assisted backscattering where DF relaying is considered. **Topology 3 (T3)**: UE-assisted backscattering, where both UE-assisted uplink transmission T3(a), and UE-assisted downlink transmission T3(b) are shown.

2) T1(b): Frequency Division Duplex (FDD): In this case, the forward and backward channels are uncorrelated, with FDD transmission being assumed[3]. This scenario corresponds to practical techniques proposed in the literature for backscatter communications, where the A-IoT device shifts the frequency of the backscattered signal to avoid direct link interference, as discussed in [35]. In this paper, we assume that the forward and backward channels are independent. Therefore, from (1), the SNR at the BS can be expressed as

$$\gamma_b^{\mathrm{T1(b)}} = \frac{\alpha P \left|h_{ab}\right|^2 \left|h_{ba}\right|^2}{\sigma_o^2}. \tag{3}$$

B. Topology 2 (T2): Relay-Assisted Backscattering

We consider a DF relaying protocol, where the transmission is accomplished in two phases. In the first phase, the half-duplex relay illuminates the A-IoT device with a carrier signal s, and the backscattered signal is received at both the relay and the BS. In the second phase, the relay forwards the signal to the BS, depending on the decoding state at the relay node in the first phase. Specifically, selection DF relaying is considered [39], [40]. The relay sends information to the BS only if it successfully decodes the symbol in the first phase; otherwise, it remains idle. Thus, in the first phase, the received signals at the relay and the BS are expressed, respectively, as

$$y_{r,1} = \sqrt{\alpha P} h_{ar} h_{ra} c s + n_r, \tag{4}$$

$$y_{b,1} = \sqrt{P} h_{rb} s + \sqrt{\alpha P} h_{ab} h_{ra} c s + n_b, \tag{5}$$

where $n_r \sim \mathcal{CN}(0, \sigma_o^2)$ and $n_b \sim \mathcal{CN}(0, \sigma_o^2)$ are the AWGN components at the relay and BS, respectively. From (4), considering symmetric channels, the SNR at the relay is given as

$$\gamma_r^{\mathrm{T2}} = \frac{\alpha P \left|h_{ra}\right|^4}{\sigma_o^2}. \tag{6}$$

[3]The work in [38] demonstrated the implementation of a single-antenna FDD reader that is compatible with ultrahigh frequency RFID systems.

Since the carrier signal is predefined and the channel state information (CSI) h_{rb} is assumed to be available at the BS, the received carrier term $\sqrt{P} h_{rb} s$ in (5) can be removed via SIC before decoding c. Hence, the SNR at the BS in the first phase can be expressed as

$$\gamma_{b,1}^{\mathrm{T2}} = \frac{\alpha P \left|h_{ab}\right|^2 \left|h_{ra}\right|^2}{\sigma_o^2}. \tag{7}$$

In the second phase, if the relay correctly decoded the backscattered signal in the first phase, it forwards the decoded information to the BS, and the received signal is given as

$$y_{b,2} = \sqrt{P} h_{rb} c + n_b. \tag{8}$$

The SNR at the BS in the second phase is given as

$$\gamma_{b,2}^{\mathrm{T2}} = \frac{P \left|h_{rb}\right|^2}{\sigma_o^2}. \tag{9}$$

C. Topology 3 (T3): UE-Assisted Backscattering

In this topology, we explore UE-assisted transmission, where the UE aids the A-IoT device in transmitting its signal to the BS. We consider two scenarios: UE-assisted uplink data transmission and UE-assisted downlink data transmission.

1) T3(a): UE-Assisted Uplink Transmission: In this scenario, the UE sends its information signal x, where $\mathbb{E}[|x^2|] = 1$, to the BS in the uplink direction. Simultaneously, it illuminates the A-IoT device, which transmits a signal c by piggybacking on the UE signal using backscatter modulation [4]. The received signal at the BS can be expressed as

$$y_b = \sqrt{P} h_{ub} x + \sqrt{\alpha P} h_{ab} h_{ua} c x + \acute{n}_b, \tag{10}$$

where $\acute{n}_b \sim \mathcal{CN}(0, \sigma_1^2)$ is the AWGN. The BS first decodes the UE signal using SIC, treating the backscatter link as interference, and the SNR for decoding x is

[4]Alternatively, the UE could send a known signal, such as a sounding reference signal (SRS), enabling the BS to employ a UE-specific channel estimator as a receiver for the A-IoT message. However, in this paper, we focus on the information transmission for both the UE and the A-IoT device.

This article has been accepted for publication in a future issue of this journal, but has not been fully edited. Content may change prior to final publication.
Citation information: DOI: 10.1109/TCCN.2025.3586219, IEEE Transactions on Cognitive Communications and Networking

$$\gamma_{b,x}^{\mathrm{T3(a)}} = \frac{P\left|h_{ub}\right|^2}{\alpha P\left|h_{ab}\right|^2\left|h_{ua}\right|^2 + \sigma_1^2}. \tag{11}$$

After decoding the UE signal x, the BS can decode the backscattered signal c by removing the first term in (10), and the SNR for decoding c is

$$\gamma_{b,c}^{\mathrm{T3(a)}} = \frac{\alpha P\left|h_{ab}\right|^2\left|h_{ua}\right|^2}{\sigma_o^2}. \tag{12}$$

It should be noted that the noise variance employed for decoding the UE signal x is denoted as σ_1^2, which is greater than σ_o^2, the noise variance used for decoding the signal c. In fact, we define the noise variance in terms of the bandwidth, as will be discussed in Section IV, considering that the A-IoT device signal typically utilizes significantly less bandwidth compared to the UE signal.

2) T3(b): UE-Assisted Downlink Transmission: In this scenario, The BS sends the information signal x to the UE while simultaneously illuminating the A-IoT device to modulate its signal c. The received signal at the UE is expressed as

$$y_u = \sqrt{P}h_{bu}x + \sqrt{\alpha P}h_{au}h_{ba}cx + n_u, \tag{13}$$

where $n_u \sim \mathcal{CN}(0, \sigma_1^2)$. The UE first decodes its own signal by treating the backscatter link as interference. Thus, the SNR for decoding x is derived as

$$\gamma_{u,x}^{\mathrm{T3(b)}} = \frac{P\left|h_{bu}\right|^2}{\alpha P\left|h_{au}\right|^2\left|h_{ba}\right|^2 + \sigma_1^2}. \tag{14}$$

After decoding x and removing the first term in (13) using the SIC technique, the UE decodes the backscattered signal c, where the SNR is given as

$$\gamma_{u,c}^{\mathrm{T3(b)}} = \frac{\alpha P\left|h_{au}\right|^2\left|h_{ba}\right|^2}{\sigma_o^2}. \tag{15}$$

The UE then modulates and sends the decoded signal c to the BS, and the received signal at the BS is given by

$$y_b = \sqrt{P}h_{ub}c + n_b. \tag{16}$$

The SNR for decoding c at the BS is then given by

$$\gamma_{b,c}^{\mathrm{T3(b)}} = \frac{P\left|h_{ub}\right|^2}{\sigma_o^2}. \tag{17}$$

III. Outage Performance Analysis

In this section, we characterize the performance of the different topologies presented in Section II in terms of outage probability. An outage event of any topology occurs when the transmission rate falls below a specific target threshold. We derive closed-form expressions of the outage probability of each topology. Additionally, to facilitate comparison, we conduct an asymptotic analysis and evaluate the diversity order of each topology.

A. Topology 1 (T1): Direct Connection with the BS

In this topology, we consider a target rate for the A-IoT device, denoted as R_o, and the achievable rate is expressed as

$$R^{\hat{\tau}} = \log_2(1 + \gamma_b^{\hat{\tau}}), \tag{18}$$

where $\hat{\tau} \in \{\mathrm{T1(a)}, \mathrm{T1(b)}\}$.

1) T1(a): Full-Duplex Receiver with Channel Reciprocity: In this case, the outage probability is expressed as

$$\begin{aligned} P_{out}^{\mathrm{T1(a)}} &= \Pr[R^{\mathrm{T1(a)}} < R_o] \\ &= \Pr[\left|h_{ba}\right|^4 < \theta_1], \end{aligned} \tag{19}$$

where $\theta_1 \triangleq \frac{2^{R_o}-1}{\alpha\gamma_o}$, and $\gamma_o \triangleq \frac{P}{\sigma_o^2}$ is the transmit SNR. The outage probability is derived in the following lemma.

Lemma 1. *The outage probability for T1(a) is given by*

$$P_{out}^{\mathrm{T1(a)}} = 1 - e^{-\frac{\sqrt{\theta_1}}{\beta_{ba}}}. \tag{20}$$

Proof: Note that $\left|h_{ba}\right|^2 \sim \exp(\frac{1}{\beta_{ba}})$. Using the transformation of random variables identities, the CDF of the random variable $\left|h_{ba}\right|^4$ is given by $F_{|h_{ba}|^2}(x) = 1 - e^{-\frac{\sqrt{x}}{\beta_{ba}}}$. Substituting this result into (19) gives (20). □

Corollary 1. At high SNR γ_o, the asymptotic expression for the outage probability of T1(a) is given as

$$P_{out,\infty}^{\mathrm{T1(a)}} = \frac{\sqrt{\theta_1}}{\beta_{ba}} \tag{21}$$

Proof: Note that as $\gamma_o \to \infty$, $\theta_1 \to 0$. Therefore, (21) can be easily obtained from (20) by using the approximation $e^x \approx 1 + x$ for small values of x. □

It can be inferred from (21) that, at high SNR, the outage probability scales as $1/\sqrt{\gamma_o}$, indicating a diversity order of $\frac{1}{2}$.

2) T1(b): Frequency Division Duplex (FDD) : In this case, from (18), the outage probability is expressed as

$$\begin{aligned} P_{out}^{\mathrm{T1(b)}} &= \Pr[R^{\mathrm{T1(b)}} < R_o] \\ &= \Pr\Big[\left|h_{ab}\right|^2\left|h_{ba}\right|^2 < \theta_1\Big]. \end{aligned} \tag{22}$$

The outage probability is derived in the following lemma.

Lemma 2. *The outage probability for T1(b) is given as*

$$P_{out}^{\mathrm{T1(b)}} = 1 - \sqrt{\frac{4\theta_1}{\beta_{ab}\beta_{ba}}}K_1\Big(\sqrt{\frac{4\theta_1}{\beta_{ab}\beta_{ba}}}\Big), \tag{23}$$

where $K_v(z)$ is the modified Bessel function of the second kind [41, Eq. (8.407.1)].

Proof: See Appendix A. □

Corollary 2. At high SNR, the asymptotic expression for the outage probability of T1(b) is given as

$$P_{out,\infty}^{\mathrm{T1(b)}} = -\frac{\theta_1}{\beta_{ab}^2}\ln\Big(\frac{\theta_1}{\beta_{ab}^2}\Big). \tag{24}$$

This article has been accepted for publication in a future issue of this journal, but has not been fully edited. Content may change prior to final publication.
Citation information: DOI: 10.1109/TCCN.2025.3586219, IEEE Transactions on Cognitive Communications and Networking

Proof: Using the approximation of $K_1(x)$ as $x \to 0$, we have $K_1(x) \approx \frac{1}{x}+\frac{x}{2}\ln(\frac{x}{2})$ [42]. Therefore, $1 - xK_1(x) \approx -\frac{x^2}{2}\ln(\frac{x}{2}) = -\frac{x^2}{4}\ln(\frac{x^2}{4})$. Applying this result in (23) as $\gamma_0 \to \infty$ (or equivalently $\theta_1 \to 0$) gives (24). □

To gain additional insights, we investigate the diversity order in the following analysis. According to [43], the diversity order of topology τ is defined as

$$d_\tau = -\lim_{\gamma_0 \to \infty} \frac{\log(P^{\tau}_{out,\infty})}{\log(\gamma_0)}. \tag{25}$$

Corollary 3. The diversity order of the A-IoT device with topology T1(b) is given as

$$d_{\mathrm{T1(b)}} = 1. \tag{26}$$

Proof: This result can be obtained using (24) and (25). □

B. Topology 2 (T2): Relay-Assisted Backscattering

Considering the half-duplex operation of the relay, the achievable rate of the A-IoT device with this topology is given by

$$R^{\mathrm{T2}} = \begin{cases} \frac{1}{2}\log_2(1+\gamma^{\mathrm{T2}}_{b,1}) & \gamma_r < 2^{2R_o}-1 \\ \frac{1}{2}\log_2(1+\gamma^{\mathrm{T2}}_{b,1}+\gamma^{\mathrm{T2}}_{b,2}) & \gamma_r \geq 2^{2R_o}-1 \end{cases} \tag{27}$$

The first case in (27) corresponds to the relay being unable to decode the signal in the first phase. The second case corresponds to the relay successfully decoding and forwarding the A-IoT signal; in this case, the SNR of the combined maximum ratio combining (MRC) signal at the BS is the sum of the received SNRs during the first and second phases of transmission [44]. From (27), the outage event occurs either when the relay fails to decode and the A-IoT device-BS link is in outage, *or* when the relay successfully decodes, but both the A-IoT device-BS link and relay-BS link are in outage. Thus, the outage probability is expressed as

$$\begin{aligned} P^{\mathrm{T2}}_{out} &= \Pr\Big[R^{\mathrm{T2}} < R_o\Big] \\ &= \Pr\Big[\gamma^{\mathrm{T2}}_r < 2^{2R_o}-1\Big]\Pr\Big[\gamma^{\mathrm{T2}}_{b,1} < 2^{2R_0}-1\Big] \\ &+ \Pr\Big[\gamma^{\mathrm{T2}}_r \geq 2^{2R_o}-1\Big]\Pr\Big[\gamma^{\mathrm{T2}}_{b,1}+\gamma^{\mathrm{T2}}_{b,2} < 2^{2R_0}-1\Big]. \end{aligned} \tag{28}$$

The expression for the outage probability of T2 is given in the following lemma.

Lemma 3. *The outage probability of T2 is given as*

$$\begin{aligned} P^{\mathrm{T2}}_{out} &= \Big(1-e^{-\frac{\sqrt{\theta_2}}{\beta_{ra}}}\Big)\Big(1-\sqrt{\tfrac{4\theta_2}{\beta_{ab}\beta_{ra}}}K_1\Big(\sqrt{\frac{4\theta_2}{\beta_{ab}\beta_{ra}}}\Big)\Big) \\ &+ \Big(e^{-\frac{\sqrt{\theta_2}}{\beta_{ra}}}\Big)\Big[1-\sqrt{\tfrac{4\theta_2}{\beta_{ab}\beta_{ra}}}K_1\Big(\sqrt{\tfrac{4\theta_2}{\beta_{ab}\beta_{ra}}}\Big) - \frac{2e^{-\frac{\alpha\theta_2}{\beta_{rb}}}}{\beta_{ab}\beta_{ra}} \\ &\times \Big(\frac{\pi\theta_2}{2N}\sum_{j=0}^{N} e^{\frac{\alpha\theta_2(\phi_j+1)}{2\beta_{rb}}}K_0\Big(\sqrt{\tfrac{4\theta_2(\phi_j+1)}{2\beta_{ab}\beta_{ra}}}\Big)\sqrt{1-\phi_j^2}\Big)\Big], \end{aligned} \tag{29}$$

where $\theta_2 \triangleq \frac{2^{2R_o}-1}{\alpha\gamma_o}$, $\phi_j \triangleq \cos[(2j-2)\pi/(2N)]$, and N is an accuracy-complexity tradeoff parameter.

Proof: See Appendix B. □

Corollary 4. At high SNR, the asymptotic outage probability of T1(a) given in (29) is expressed as

$$\begin{aligned} P^{\mathrm{T2}}_{out,\infty} &= \Big(1-e^{-\frac{\sqrt{\theta_2}}{\beta_{ra}}}\Big)\Big(1-\sqrt{\tfrac{4\theta_2}{\beta_{ab}\beta_{ra}}}K_1\Big(\sqrt{\tfrac{4\theta_2}{\beta_{ab}\beta_{ra}}}\Big)\Big) \\ &= \Big(\frac{\sqrt{\theta_2}}{\beta_{ra}}\Big)\Big(-\frac{\theta_1}{\beta_{ab}\beta_{ra}}\ln\Big(\frac{\theta_2}{\beta_{ab}\beta_{ra}}\Big)\Big). \end{aligned} \tag{30}$$

Proof: The first equality in (30) is obtained as the second term in (29) approaches zero when $\gamma_o \to \infty$. The second equality can be derived using the approximation $e^x \approx 1+x$ when $x \to 0$, and the approximation $1-xK_1(x) \approx -\frac{x^2}{4}\ln(\frac{x^2}{4})$ as discussed in the proof of **Corollary 2**. □

Corollary 5. The diversity order of the A-IoT device with T2 is

$$d_{\mathrm{T2}} = \frac{3}{2}. \tag{31}$$

Proof: This result can be obtained using (25) and (30). □

Remark 1. It follows from **Corollary 1** that the asymptotic outage probability of T1(a) scales as $P^{\mathrm{T1(a)}}_{out,\infty} \propto \frac{1}{\gamma_o^{1/2}}$. Moreover, from **Corollary 2** and **Corollary 3** we find that the asymptotic outage probability of T1(b) scales as $P^{\mathrm{T1(b)}}_{out,\infty} \propto \frac{1}{\gamma_o}$. This indicates that T1(b) offers superior asymptotic performance compared to T1(a). Conversely, according to **Corollary 5**, $P^{\mathrm{T2}}_{out,\infty} \propto \frac{1}{\gamma_o^{3/2}}$, suggesting that T2 achieves a higher diversity order than both T1(a) and T1(b). However, it should be highlighted that although T2 employs two paths between the A-IoT device and the BS, the achieved diversity order is less than two. This can be explained by the operational differences from the conventional DF protocol, as discussed in [39], which achieves a diversity order of two. Specifically, in the first phase of T2, the relay intercepts the A-IoT signal via a round-trip path, and the received signal at the BS is subject to the effects of two multiplicative channels, which impacts the overall performance.

C. Topology 3 (T3): UE-Assisted Backscattering

In this topology, the SIC technique is applied at the receiver to decode both the UE signal x and the A-IoT signal c. Since x is decoded first, the probability of an outage event when decoding c depends on the outage conditions of both the UE and AIoT signals. In the following analysis, in addition to the designated target rate R_o for A-IoT device transmissions, a specific target rate R_1 is also established for UE transmissions. First, we investigate the outage probability for the A-IoT signal in both T3(a) and T3(b). Then, we examine the outage probability of the UE signal within the context of T3(a).

1) T3(a): UE-Assisted Uplink Transmission: According to the SIC principle, an outage event of the AIoT signal occurs when the BS fails to decode either the UE signal or the A-IoT signal, and the outage probability can be expressed as

This article has been accepted for publication in a future issue of this journal, but has not been fully edited. Content may change prior to final publication.
Citation information: DOI: 10.1109/TCCN.2025.3586219, IEEE Transactions on Cognitive Communications and Networking

$$P_{out,c}^{\mathrm{T3(a)}} = 1-\Pr\Big[\gamma_{b,x}^{\mathrm{T3(a)}} \geq 2^{R_1}-1,\, \gamma_{b,c}^{\mathrm{T3(a)}} \geq 2^{R_o}-1\Big]. \tag{32}$$

Lemma 4. *The outage probability of the A-IoT signal in T3(a) is given as*

$$P_{out,c}^{\mathrm{T3(a)}} = 1 - e^{-\frac{\theta_3}{\beta_{ub}}}\Bigg[\sqrt{\frac{\beta_{ub}}{\rho\beta_{ab}\beta_{ua}}}e^{\frac{\beta_{ub}}{2\rho\beta_{ab}\beta_{ua}}}W_{-\frac{1}{2},0}\Big(\frac{\beta_{ub}}{\rho\beta_{ab}\beta_{ua}}\Big) - \frac{\pi\theta_1}{N\beta_{ab}\beta_{ua}}\sum_{j=0}^{N} e^{\frac{\rho\theta_1(\phi_j+1)}{2\beta_{ua}}}K_0\Big(2\sqrt{\frac{\theta_1(\phi_j+1)}{2\beta_{ab}\beta_{ua}}}\Big)\sqrt{1-\phi_j^2}\Bigg]. \tag{33}$$

Proof: See Appendix C. □

Corollary 6. At high SNR, the asymptotic expression for the outage probability given in (33) is expressed as

$$P_{out,c,\infty}^{\mathrm{T3(a)}} = -\frac{\pi\theta_1}{N\beta_{ab}\beta_{ua}}\sum_{j=0}^{N}\ln\Big(2\sqrt{\frac{\theta_1(\phi_j+1)}{2\beta_{ab}\beta_{ua}}}\Big)\sqrt{1-\phi_j^2} \tag{34}$$

Proof: The result can be obtained using the high SNR approximation principles and using the identity $K_0(x) \approx -\ln(x)$ [45, Eq. (10.30.3)]. Moreover, the first term inside the bracket in (33) is equal to one since $\sqrt{x}e^{x/2}W_{-\frac{1}{2},0}(x) \to 1$ for sufficiently high x [46]. Incorporating these results into (33) gives (34). □

2) T3(b): UE-Assisted Downlink Transmission : In this topology, an outage event occurs either when the UE fails to decode either the BS signal or the A-IoT signal, *or* when the UE decodes both signals correctly but the BS fails to decode UE signal transmitted in the second phase. Thus, the outage event can be described as follows

$$\begin{aligned}&\Big[\{\gamma_{u,x}^{\mathrm{T3(b)}} < 2^{R_o}-1\}\cup\{\gamma_{u,c}^{\mathrm{T3(b)}} < 2^{2R_o}-1\}\Big]\\ \cup&\Big[\{\gamma_{u,x}^{\mathrm{T3(b)}} \geq 2^{R_o}-1\}\cap\{\gamma_{u,c}^{\mathrm{T3(b)}} < 2^{2R_o}-1\}\\ &\cap\{\gamma_{b,c}^{\mathrm{T3(b)}} < 2^{2R_o}-1\}\Big]\end{aligned} \tag{35}$$

Accordingly, the outage probability can be expressed as

$$\begin{aligned}P_{out,c}^{\mathrm{T3(b)}} =& 1-\Pr\Big[\gamma_{u,x}^{\mathrm{T3(b)}} \geq 2^{R_1}-1,\, \gamma_{u,c}^{\mathrm{T3(b)}} \geq 2^{2R_o}-1\Big]\\ &+\Pr\Big[\gamma_{u,x}^{\mathrm{T3(b)}} \geq 2^{R_1}-1,\, \gamma_{u,c}^{\mathrm{T3(b)}} \geq 2^{2R_o}-1\Big]\\ &\times\Pr\Big[\gamma_{b,c}^{\mathrm{T3(b)}} < 2^{2R_o}-1\Big]\end{aligned} \tag{36}$$

Lemma 5. *The outage probability of the A-IoT device in T3(b) is given as*

$$P_{out,c}^{\mathrm{T3(b)}} = 1 - e^{-\frac{2\theta_3}{\beta_{bu}}}\Bigg[\sqrt{\frac{\beta_{bu}}{\rho\beta_{au}\beta_{ba}}}e^{\frac{\beta_{bu}}{2\rho\beta_{au}\beta_{ba}}}W_{-\frac{1}{2},0}\Big(\frac{\beta_{bu}}{\rho\beta_{au}\beta_{ba}}\Big) - \frac{\pi\theta_2}{N\beta_{au}\beta_{ba}}\sum_{j=0}^{N} e^{\frac{\rho\theta_2(\phi_j+1)}{2\beta_{ba}}}K_0\Big(2\sqrt{\frac{\theta_2(\phi_j+1)}{2\beta_{au}\beta_{ba}}}\Big)\sqrt{1-\phi_j^2}\Bigg] \tag{37}$$

where $W_{a,b}(z)$ is the Whittaker function [41, Eq. (9.220.4)].

Proof: See Appendix D. □

Corollary 7. At high SNR, the asymptotic expression for the outage probability given in (37) is expressed as

$$P_{out,c,\infty}^{\mathrm{T3(b)}} = -\frac{\pi\theta_1}{N\beta_{au}\beta_{ba}}\sum_{j=0}^{N}\ln\Big(2\sqrt{\frac{\theta_2(\phi_j+1)}{2\beta_{au}\beta_{ba}}}\Big)\sqrt{1-\phi_j^2} \tag{38}$$

Proof: The result stated in (38) can be proved using a method analogous to the one applied in the proof of **Corollary 6**. □

Corollary 8. The diversity order of the A-IoT signal for T3(a) and T3(b) are

$$d_{\mathrm{T3(a)}} = d_{\mathrm{T3(b)}} = 1. \tag{39}$$

Proof: From (25), (34), and (38), it can be shown that each term in the summations in (34) and (38) has a diversity order of one. Therefore, the overall weighted sum, which is a sum of such terms, will exhibit a similar trend in its behavior as $\gamma_o \to \infty$; thus, we obtain (39). □

3) Outage Probability of UE in T3(a): While the main focus in this paper is on the A-IoT system, T3 includes both UE and A-IoT signals. Thus, in this subsection, we derive the the outage probability of the UE's signal x to examine how A-IoT transmission affects the UE performance. The outage probability is given by

$$P_{out,x}^{\mathrm{T3(a)}} = \Pr\Big[\gamma_{b,x}^{\mathrm{T3(a)}} < 2^{R_1}-1\Big]. \tag{40}$$

Lemma 6. *The outage probability of the UE signal in T3(a) is given by*

$$P_{out,x}^{\mathrm{T3(a)}} = 1 - \frac{2e^{-\frac{\theta_3}{\beta_{ub}}}}{\beta_{ab}\beta_{ua}}\sqrt{\frac{\beta_{ab}\beta_{ua}\beta_{ub}}{4\rho}}e^{\frac{\beta_{ub}}{2\rho\beta_{ab}\beta_{ua}}}W_{-\frac{1}{2},0}\Big(\frac{\beta_{ub}}{\rho\beta_{ab}\beta_{ua}}\Big). \tag{41}$$

Proof: See Appendix E. □

Corollary 9. At high SNR, the asymptotic expression for the outage probability given in (41) and the diversity order are, respectively, given by

$$P_{out,x,\infty}^{\mathrm{T3(a)}} = 1 - \frac{2}{\beta_{ab}\beta_{ua}}\sqrt{\frac{\beta_{ab}\beta_{ua}\beta_{ub}}{4\rho}}e^{\frac{\beta_{ub}}{2\rho\beta_{ab}\beta_{ua}}}W_{-\frac{1}{2},0}\Big(\frac{\beta_{ub}}{\rho\beta_{ab}\beta_{ua}}\Big), \tag{42}$$

$$d_{\mathrm{T3(a)},x} = 0. \tag{43}$$

Proof: Equation (42) can be easily derived using high SNR approximation principles, and (43) follows from (25) and (42). □

Remark 2. From **Corollary 9**, we observe the following: 1) the outage probability of the UE approaches a fixed value at high SNR, indicating the presence of error floors that affect the diversity order; 2) the outage probability of the UE increases with α. On the other hand, from **Corollaries 1, 2, 4, 6,** and **7**, we see that in the high SNR regime, the outage probability of the A-IoT signal decreases with α.

This article has been accepted for publication in a future issue of this journal, but has not been fully edited. Content may change prior to final publication.
Citation information: DOI: 10.1109/TCCN.2025.3586219, IEEE Transactions on Cognitive Communications and Networking

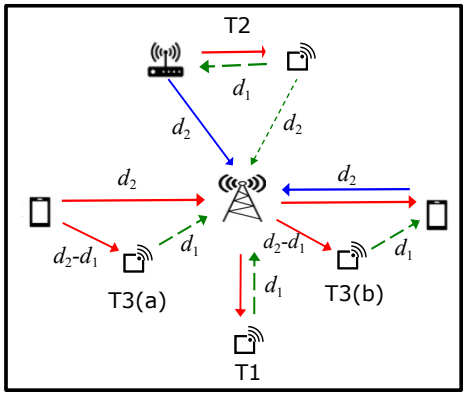

Fig. 2. Illustration of the simulation configuration indicating the distances of the different links for all topologies.

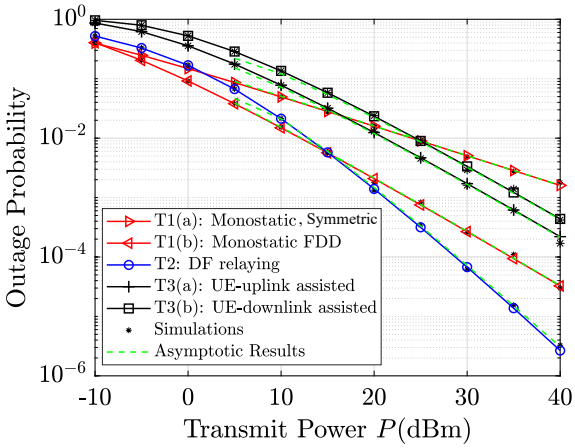

Fig. 3. Outage probability versus the transmit power P for the different topologies.

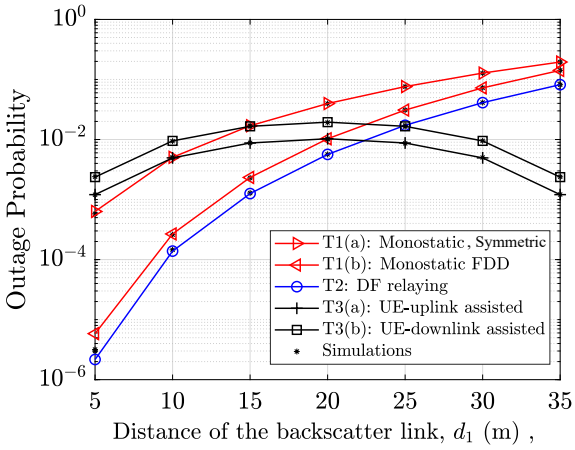

Fig. 4. Outage probability versus the distance of the backscatter link d_1, for the different topologies, with $d_2 = 40$m.

IV. Numerical Results and Discussions

In this section, we evaluate and compare the performance of different A-IoT topologies using both analytical expressions and Monte Carlo simulations. We also discuss practical considerations and potential extensions within the broader context of emerging A-IoT research.

A. Numerical results

In this subsection, we numerically evaluate the performance of the proposed schemes considering 10^6 Monte Carlo trials to verify the analytical results. Unless otherwise stated, we set P = 30 dBm, $\alpha = 0.5$, $R_o = 0.2$ bps/Hz and $R_1 = 1$ bps/Hz. We define the noise variances as a function of the bandwidth: $\sigma_o^2 = N_o B_o$, and $\sigma_1^2 = N_o B_1$, where $N_o = -174\,\text{dBm/Hz}$ is the thermal noise power spectral density [3], $B_o = 10\,\text{kHz}$, and $B_1 = 1.4\,\text{MHz}$ [47]. The channel gain $\beta_{ij} = \Omega d_{ij}^{-\vartheta}$, where $\Omega = (\frac{3\times10^8}{4\pi f})^2$ is the average channel attenuation at unit reference distance with $f = 915\text{MHz}$ [5] as the transmit frequency, d_{ij} is the distance between the nodes i and j, and $\vartheta = 3$ is the path loss exponent.

For a fair comparison, the distances between the different nodes are considered as in Fig. 2. The parameter d_1 represents the distance of the backscatter link, and is kept identical across all topologies. Unless otherwise stated, we set $d_1 = 10\text{m}$, and $d_2 = 3d_1$. In the T3 configuration, the A-IoT device is positioned between the BS and the UE. In contrast, in the T2 configuration, the A-IoT device is typically located near the relay node. As a result, both the relay and the A-IoT device are situated at a distance d_2 from the BS. Additionally, T2 includes a direct backscatter link between the A-IoT device and the BS.

Figure 3 illustrates the outage probability versus P. The analytical and simulation results are in close agreement, and the asymptotic results validate the expected high-SNR behavior. As P increases, the outage probability decreases across all topologies, indicating improved reliability. The derived diversity orders—$\frac{1}{2}$, 1, $\frac{3}{2}$, 1, and 1 for T1(a), T1(b), T2, T3(a), and T3(b), respectively—are clearly reflected in the simulation trends. At practical power levels (e.g., above 15 dBm), T2 exhibits the best performance due to its superior diversity, as discussed in Remark 1. T1(b) offers a compelling balance between diversity and hardware simplicity, making it a promising candidate for practical A-IoT deployments. T3(a) outperforms T3(b), which is constrained by the half-duplex operation at the UE. T1(a) shows the weakest performance at high SNR, primarily due to limited power scaling. It is also worth noting that the performance of T3 is more sensitive to the relative placement of the A-IoT device to surrounding nodes—a factor that will be further explored in Fig. 4.

Figure 4 shows the outage probability as a function of the backscatter link distance d_1, with d_2 fixed at 40 m. For T1 and T2, the performance degrades as d_1 increases, with T2 consistently outperforming T1(a) and T1(b) across all distances. At larger d_1, the performance gap narrows, indicating convergence in their reliability. In contrast, T3 exhibits a non-monotonic trend. At short distances ($d_1 \leq 10\,\text{m}$), T3 shows the poorest performance among all topologies. However, as d_1 increases beyond $10\,\text{m}$, its performance improves and eventually surpasses the others. This is due to the decreasing $d_2 - d_1$ separation (as shown in Fig. 2), which brings the A-IoT device closer to the source signal, effectively forming a bistatic backscatter setup with stronger illumination. Thus, UE-assisted backscattering is particularly effective at longer backscatter link distance d_1. It is also worth noting that T1(b) achieves performance comparable to T2 across the full range

This article has been accepted for publication in a future issue of this journal, but has not been fully edited. Content may change prior to final publication.
Citation information: DOI: 10.1109/TCCN.2025.3586219, IEEE Transactions on Cognitive Communications and Networking

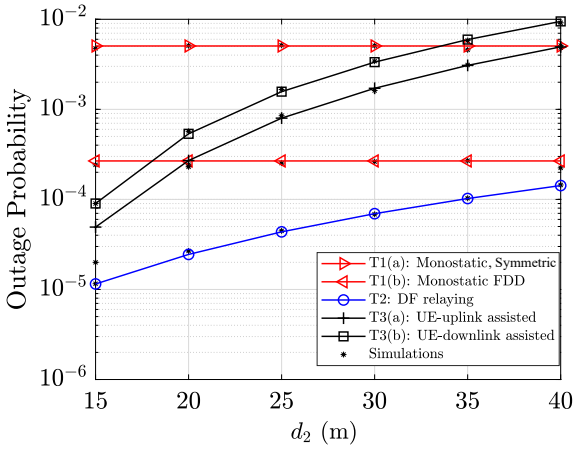

Fig. 5. Outage probability versus the distance d_2, where $P = 30$dBm, and $d_1 = 10$m.

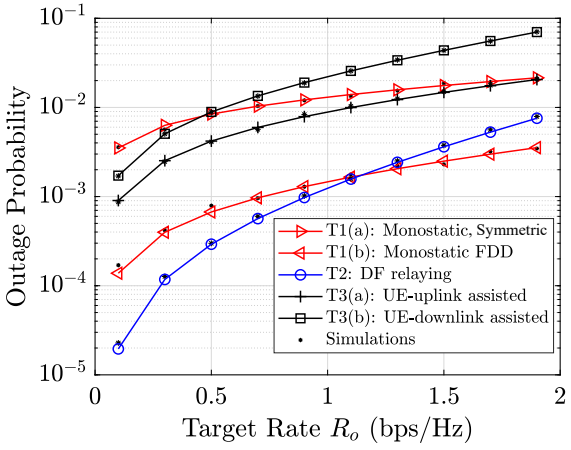

Fig. 7. Outage probability against R_o for the different topologies, with $R_1 = 2$ bps/Hz .

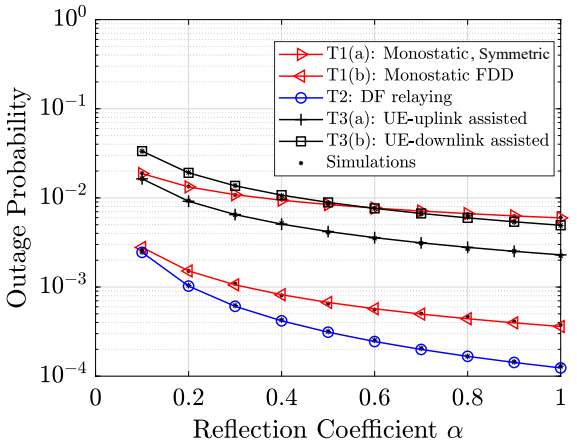

Fig. 6. Outage probability against the reflection coefficient α for the different topologies.

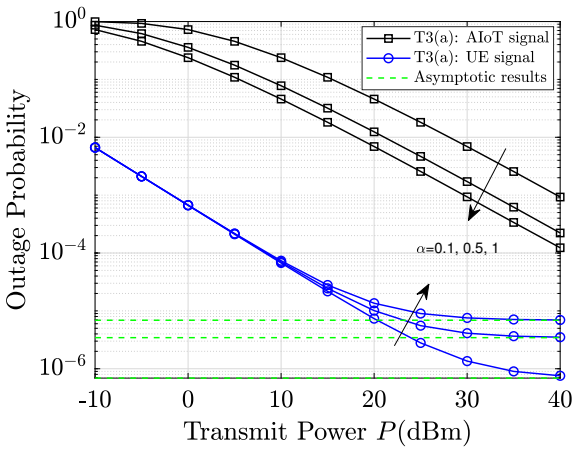

Fig. 8. Outage probability against transmit power P for different values of α, with $R_o = 0.2$ bps/Hz, and $R_1 = 2$ bps/Hz.

of backscatter distances, highlighting its potential as a simpler yet effective alternative.

Figure 5 illustrates the outage probability versus the distance d_2, with d_1 fixed at 10 m. T2 consistently outperforms all other topologies across the entire d_2 range. Moreover, the rate of performance degradation associated with T2 is significantly lower compared to that observed with T3, highlighting its robustness—primarily due to the active transmission capabilities at the relay node. In contrast, T1(a) and T1(b) remain unaffected by changes in d_2, as their performance depends solely on d_1.

The outage probability versus the reflection coefficient α for the different topologies is plotted in Fig. 6. The performance of all topologies improves as the reflection coefficient increases, consistent with the aforementioned analysis. Additionally, it is shown that at $\alpha = 0.1$, both T1(b) and T2 exhibit similar performance. However, as α increases, a noticeable performance gap emerges, with T2 outperforming T1(b), highlighting the influence of α on their relative performance. The same observation applies to T1(a) and T3(a).

Figure 7 shows the outage probability as a function of the target rate R_o. As expected, reducing R_o improves the outage performance across all topologies. At low rates (e.g., $R_o \leq 1.1$ bps/Hz), T2 achieves the best performance. However, its performance declines more rapidly with increasing R_o, due to the spectral efficiency loss introduced by half-duplex relaying. At higher rates, T1(b) becomes more efficient than T2. The performance of T3(b) also degrades sharply at higher R_o, attributed to the overhead of its two-phase UE-assisted forwarding. Note also that T3(a) outperforms T1(a) at low rates, but their performance converges as R_o increases, indicating a reduced performance gap. This suggests that the optimal topology depends on the operating rate and the system's tolerance to complexity and spectral efficiency trade-offs.

While this paper primarily focuses on the outage performance of A-IoT backscatter transmission, Fig. 8 examines its impact on the performance of the primary UE in T3(a). The figure shows the outage probabilities of both the UE and A-IoT signals versus the transmit power P for different values of the backscatter coefficient α. As expected, the UE consistently outperforms the A-IoT signal due to the latter's passive nature. Two key observations arise under parasitic communication, where the backscatter signal acts as interference to the UE. First, the UE signal exhibits an error floor at high SNR, as discussed in Remark 2. Second, a trade-off emerges:

This article has been accepted for publication in a future issue of this journal, but has not been fully edited. Content may change prior to final publication.
Citation information: DOI: 10.1109/TCCN.2025.3586219, IEEE Transactions on Cognitive Communications and Networking

increasing α improves A-IoT performance but degrades UE performance, especially at high SNR. This suggests future work could explore optimizing α to meet quality of service (QoS) requirements for both links. It is also noted that the outage probability of the UE in T3(b) mirrors that in T3(a), owing to their symmetric configurations. Therefore, Fig. 8 focuses exclusively on T3(a).

It is worth noting that there are two main SR setups, depending on the relative symbol durations of the primary and backscatter systems. In the commensal SR, where the backscatter symbol duration is much longer, the backscattered signal can enhance the primary transmission as an additional multipath component. In contrast, the parasitic SR assumes similar symbol durations, causing the backscatter signal to act as interference. In this paper, we adopt the parasitic SR model [26]–[31], [48], as our main objective is to evaluate the outage performance of the A-IoT system. Although this setup may degrade the primary system at high SNR, the effect can be controlled by tuning the reflection coefficient, as shown in Fig. 8. Notably, the parasitic setup is expected to provide better outage performance for A-IoT compared to the commensal case. This is because the commensal model requires a much longer A-IoT symbol duration, which reduces the spectral efficiency. Consequently, for a given target rate, the outage performance of the A-IoT system in the commensal configuration is typically worse. Investigating the trade-off between these two SR modes in the A-IoT context is a promising direction for future research.

B. Practical Considerations and Future Extensions

In this subsection, we address several practical aspects and open issues related to the discussed A-IoT topologies. These include energy harvesting considerations, interference management, channel estimation strategies, and emerging techniques relevant to A-IoT systems.

1) Energy Harvesting : In this study, the energy harvesting model is excluded from the outage analysis for two reasons. First, our main objective is to compare the performance of the different topologies, and including an explicit energy harvesting model would significantly complicate the analysis without altering the key comparative insights. Second, even if such a model were considered—by adding equivalent terms to the outage probability expressions—it would not affect the relative performance comparison, as it would impact all topologies equally.

Nonetheless, energy harvesting remains a fundamental enabler for battery-free A-IoT device operation. In fact, the efficiency of harvesting depends not only on ambient energy sources—such as RF signals, light, motion, or thermal gradients—but also on the device's connectivity topology. In T1, devices rely primarily on RF energy from the BS. However, large distances, particularly in macro-cell deployments, often result in insufficient power levels for efficient harvesting. Supplementary sources such as solar or thermal energy can enhance feasibility. Small-cell deployments mitigate this issue by bringing the BS closer to the devices. T2 benefits from relays located near A-IoT devices, acting as strong RF energy sources and enabling reliable energy harvesting. In T3, opportunistic RF sources such as smartphones (T3a) or BS transmissions (T3b) provide energy harvesting opportunities. Although nearby UEs can deliver relatively strong RF power at close range, the availability is sporadic and proximity-dependent. Thus, T3 devices often supplement RF harvesting with solar or motion-based sources to maintain operation between communication events. A detailed study of energy harvesting models tailored to each individual topology, and their resulting impact on outage performance, remains an interesting direction for future work.

2) Interference and Scalability Considerations: In practical A-IoT deployments, devices modulate ambient signals within their antenna bandwidth, which can potentially introduce adjacent-band interference due to the dense packing of cellular frequencies. To mitigate this, integrating RF filters into A-IoT devices may be necessary, albeit at the cost of increased hardware complexity and energy consumption. Nevertheless, since the power of backscattered signals is typically much lower—by several tens of decibels—compared to active transmissions, the risk of causing harmful interference remains minimal. Furthermore, when the symbol duration is sufficiently long, as in SR setups, the backscattered signal may appear as an additional multipath component that could enhance the primary transmission performance [23]. Still, interference among adjacent backscatter devices, particularly in multi-operator environments, remains a challenge. To support large-scale deployments, it will be crucial to establish certification processes and regulations power limits aligned with 3GPP network density and spectrum usage guidelines.

Besides adjacent-band issues, co-channel and self-interference also impact system scalability and outage behavior. In monostatic topologies such as T1 and T2, the strong illumination signal can cause self-interference at the receiver, potentially masking the weak backscatter unless advanced cancellation methods are employed [36]. In dense A-IoT networks, simultaneous reflections from multiple devices sharing the same channel may lead to increased mutual interference, thereby degrading reliability. Recent work [49] has demonstrated that constructive interference can be exploited via beamforming and tag selection to enhance signal strength and reduce mutual interference in dense backscatter systems. Topologies like T2 could mitigate this through relay clustering, while T3 benefits from leveraging existing UE scheduling and filtering to reduce contention. Nonetheless, the lack of coordination among passive devices makes interference management a critical scalability concern, warranting further study to quantify its effect on outage probability under realistic network densities.

3) Channel Estimation : In this paper, we assumed that the CSI is available at the receiver. Here, we illustrate how, in practice, CSI could be obtained for each topology. In T1, the channel estimation can be done at the BS using backscattering during the training phase, where the A-IoT device modulate a predefined sequence [37]. For T3, considering similar procedure as in [23], the receiver can estimate CSI for both the primary link and the backscatter link. In practice, the CSI can be obtained through a two-step training-based estimation process. First, the A-IoT device switches its impedance to a matched (non-backscattering) state, allowing the receiver to estimate the direct primary link channel. Then, the A-IoT device switches to a fixed and known backscatter

This article has been accepted for publication in a future issue of this journal, but has not been fully edited. Content may change prior to final publication.
Citation information: DOI: 10.1109/TCCN.2025.3586219, IEEE Transactions on Cognitive Communications and Networking

state, during which the receiver measures the composite channel. By subtracting the previously estimated direct-link component from the composite measurement, the receiver obtains the backscatter link channel. For T2, the relay (acting as a monostatic reader) can similarly estimate the relay–device channel as in T1, while the relay–BS link is obtained through conventional channel estimation on the active relay link. If a direct device–BS (bistatic) link exists, the BS can estimate it by using pilot training sent from the relay and following similar procedure described for T3, to infer the bistatic multiplicative link. It is worth mentioning also that in T3, SR setups that exploit legacy reference signals (e.g., LTE-CRS or SRS) allow receivers to decode A-IoT signals via their channel estimators [35], enabling seamless integration of A-IoT into existing cellular infrastructure eliminating the need for dedicated backscatter receiver or additional hardware in BS or mobile phone.

4) Backscatter Receiver Sensitivity: In practical deployments, the activation of A-IoT devices depends critically on the sensitivity of their wake-up radios (WuRs) or backscatter circuits. If the received signal power at the A-IoT device falls below a certain threshold, the device cannot harvest sufficient energy or detect the signal, preventing successful backscatter communication. The circuit sensitivity constraint impacts each topology differently. In T1, high path loss in macro-cell deployments may prevent activation unless WuRs with high sensitivity (e.g., below –60 dBm) are employed, or unless network densification strategies are adopted. Small-cell deployments partially mitigate this issue by reducing distances. In T2 (relay-assisted), proximity to a relay significantly improves the likelihood of satisfying the sensitivity requirement, enabling the use of ultra-low-power WuRs. In T3(a), the UE may embed a wake-up tone in its uplink, while in T3(b), the BS or a nearby UE can deliver the wake-up signal. However, variable signal strengths and potential interference must be accounted for.

For simplicity, in this study we assume that the A-IoT device receives sufficient incident power to activate its backscatter circuit. Future work could incorporate activation probability modeling to further refine outage performance evaluations under realistic sensitivity constraints.

5) Channel Modeling: In this work, we assume Rayleigh fading for all wireless links, consistent with the majority of prior works in backscatter communication [11], [20], [22]–[33], as well as the recent 3GPP A-IoT study [50]. This choice enables analytical tractability and facilitates fair performance comparison across topologies under uniform channel assumptions. While backscatter communication often involves short-range links with strong line-of-sight (LoS) components—where Rician fading may be more accurate [49]—the Rayleigh model serves as a conservative assumption, providing a worst-case performance baseline. Incorporating Rician fading as a function of the K-factor is a promising direction for future work.

6) Emerging Techniques in Backscatter Communication: In this paper, we focused on the fundamental A-IoT topologies outlined in the recent 3GPP study, as they represent practical and currently standardized deployment scenarios. Beyond these topologies, several advanced paradigms—such as cooperative backscatter systems [51], hybrid active-passive communication schemes [52], and RIS-assisted backscatter communication [52], [53]—have attracted increasing research interest. These approaches offer promising benefits, including improved link reliability, enhanced energy efficiency, and greater deployment flexibility. Extending the current analytical framework to incorporate these emerging techniques is a valuable direction for future research.

V. Conclusions

In this paper, we investigated various backscatter-based connectivity topologies for A-IoT communication, deriving the outage probability for each topology and providing a fair performance comparison. The analytical and simulation results offered valuable insights into the reliability of each topology under different system parameters and deployment conditions. Specifically, the findings show that for shorter backscatter link distances, relay-assisted backscattering (T2)—which offers performance comparable to, but generally better than, T1(b)—is preferable. In contrast, UE-assisted configurations are more effective at longer backscatter ranges. Furthermore, while T2 achieves superior performance at lower transmission rates, T1(b) outperforms T2 at higher rates due to the spectral efficiency loss introduced by the half-duplex constraint at the relay, highlighting its potential as a simpler yet effective alternative.

It is important to note that optimal topology selection depends on the specific application requirements and deployment environment. The topologies analyzed in this study represent the fundamental configurations highlighted in the recent 3GPP A-IoT study, offering a baseline for performance and diversity-order comparison. These findings can serve as a foundation for future research and system design. Potential extensions include supporting multiple A-IoT devices, exploring alternative relaying protocols such as amplify-and-forward (AF), and implementing full-duplex transmission at the relay or UE.

Appendix A
Proof of Lemma 2

Before proving (23), we introduce a useful distribution in the following proposition.

Proposition 1. If $X_1 \sim \exp(\frac{1}{\beta_1})$ and $X_2 \sim \exp(\frac{1}{\beta_2})$, then the CDF and PDF of the random variable $X \triangleq X_1 X_2$ are, respectively, given as

$$F_{X_1X_2}(x) = 1 - \sqrt{\tfrac{4x}{\beta_1\beta_2}} K_1\Big(\sqrt{\tfrac{4x}{\beta_1\beta_2}}\Big), \tag{44}$$

$$f_{X_1X_2}(x) = \frac{2}{\beta_1\beta_2} K_0\Big(\sqrt{\tfrac{4x}{\beta_1\beta_2}}\Big). \tag{45}$$

Proof: The CDF of X can be obtained as

$$\begin{aligned} F_{X_1X_2}(x) &= \Pr[X_1X_2 \le x] \\ &= \Pr[X_1 \le \frac{x}{X_2}] \\ &= \frac{1}{\beta_{ua}} \int_0^\infty (1 - e^{-\frac{x}{\beta_1 x_2}}) e^{-\frac{x_2}{\beta_2}} dx_2 \\ &= 1 - \frac{1}{\beta_2} \int_0^\infty e^{-(\frac{x}{\beta_1 x_2} + \frac{x_2}{\beta_2})} dx_2. \end{aligned} \tag{46}$$

This article has been accepted for publication in a future issue of this journal, but has not been fully edited. Content may change prior to final publication.
Citation information: DOI: 10.1109/TCCN.2025.3586219, IEEE Transactions on Cognitive Communications and Networking

Solving the last integral in (46) using [41, Eq. (3.324.1)], we obtain (44). The PDF is obtained then by differentiating (46) with respect to x as follows

$$f_{X_1X_2}(x) = \frac{1}{\beta_1\beta_2}\int_0^\infty \frac{1}{x_2} e^{-(\frac{x}{\beta_1 x_2}+\frac{x_2}{\beta_2})} dx_2 \tag{47}$$

Solving the last equation using [41, Eq. (3.471.12)], (45) is obtained. □

Now, substituting (44) in (22), (23) is obtained.

Appendix B
Proof of Lemma 3

Substituting (6), (7), and (9) into (28), the outage probability can be expressed as

$$\begin{aligned} P_{out}^{\mathrm{T2}} &= \Pr\Big[|h_{ra}|^4 < \theta_2\Big]\Pr\Big[|h_{ab}|^2|h_{ra}|^2 < \theta_2\Big] \\ &\quad + \Pr\Big[|h_{ra}|^4 \geq \theta_2\Big] \\ &\quad \times \underbrace{\Pr\Big[|h_{rb}|^2 + \alpha|h_{ab}|^2|h_{ra}|^2 < \alpha\theta_2\Big]}_{I_1}, \end{aligned} \tag{48}$$

where $\theta_2 \triangleq \frac{2^{2R_o}-1}{\alpha\gamma_o}$. As in Lemma 1, it can be shown that $\Pr\Big[|h_{ra}|^4 < \theta_2\Big] = 1 - e^{-\frac{\sqrt{\theta_2}}{\beta_{ra}}}$. Also, $\Pr\Big[|h_{ra}|^4 \geq \theta_2\Big] = e^{-\frac{\sqrt{\theta_2}}{\beta_{ra}}}$. Moreover, following a similar procedure as that in Lemma 2, it is straightforward to show that $\Pr\Big[|h_{ab}|^2|h_{ra}|^2 < \theta_2\Big] = 1 - \sqrt{\frac{4\theta_2}{\beta_{ab}\beta_{ra}}}K_1(\sqrt{\frac{4\theta_2}{\beta_{ab}\beta_{ra}}})$. Now, we find I_1, which is given as

$$\begin{aligned} I_1 &= \Pr\Big[|h_{rb}|^2 < \alpha\theta_2 - \alpha|h_{ab}|^2|h_{ra}|^2\Big] \\ &= \int_0^{\theta_2}(1 - e^{-\frac{\alpha\theta_2-\alpha x}{\beta_{rb}}}) f_{|h_{ab}|^2|h_{ra}|^2}(x)dx \\ &= 1 - \sqrt{\frac{4\theta_2}{\beta_{ab}\beta_{ra}}}K_1\Big(\sqrt{\tfrac{4\theta_2}{\beta_{ab}\beta_{ra}}}\Big) \\ &\quad - \frac{2e^{-\frac{\alpha\theta_2}{\beta_{rb}}}}{\beta_{ab}\beta_{ra}} \underbrace{\int_0^{\theta_2} e^{\frac{\alpha x}{\beta_{rb}}} K_0\Big(\sqrt{\tfrac{4x}{\beta_{ab}\beta_{ra}}}\Big)dx}_{I_2}. \end{aligned} \tag{49}$$

The integration I_2 can be solved as follows

$$\begin{aligned} I_2 &= \int_0^{\theta_2} e^{\frac{\alpha x}{\beta_{rb}}} K_0\Big(\sqrt{\tfrac{4x}{\beta_{ab}\beta_{ra}}}\Big)dx \\ &= \frac{\pi\theta_2}{2N}\sum_{j=0}^{N} e^{\frac{\alpha\theta_2(\phi_j+1)}{2\beta_{rb}}} K_0\Big(\sqrt{\tfrac{4\theta_2(\phi_j+1)}{2\beta_{ab}\beta_{ra}}}\Big)\sqrt{1-\phi_j^2} \end{aligned} \tag{50}$$

Substituting (50) into (49) and then into (48), (29) is obtained.

Appendix C
Proof of Lemma 4

Substituting (11) and (12) into (32), the outage probability can be expressed as

$$P_{out,c}^{\mathrm{T3(a)}} = 1 - \underbrace{\Pr\Big[|h_{ub}|^2 \geq (\rho|h_{ab}|^2|h_{ua}|^2 + \theta_3),\ |h_{ab}|^2|h_{ua}|^2 \geq \theta_1\Big]}_{I_3} \tag{51}$$

where $\theta_3 \triangleq \frac{2^{R_1}-1}{P/\sigma_1^2}$, and $\rho \triangleq \alpha(2^{R_1}-1)$. We find the probability I_3 as follows

$$\begin{aligned} I_3 &= \Pr\Big[|h_{ub}|^2 \geq (\rho|h_{ab}|^2|h_{ua}|^2 + \theta_3),\ |h_{ab}|^2|h_{ua}|^2 \geq \theta_1\Big] \\ &= \int_{\theta_1}^{\infty} e^{-\frac{\rho x+\theta_3}{\beta_{ub}}} f_{|h_{ab}|^2|h_{ua}|^2}(x)dx \\ &= \frac{2e^{-\frac{\theta_3}{\beta_{ub}}}}{\beta_{ab}\beta_{ua}}\int_{\theta_1}^{\infty} e^{-\frac{\rho x}{\beta_{ub}}} K_0\Big(2\sqrt{\tfrac{x}{\beta_{ab}\beta_{ua}}}\Big)dx \\ &= \frac{2e^{-\frac{\theta_3}{\beta_{ub}}}}{\beta_{ab}\beta_{ua}}\Bigg[\int_0^{\infty} e^{-\frac{\rho x}{\beta_{ub}}} K_0\Big(2\sqrt{\tfrac{x}{\beta_{ab}\beta_{ua}}}\Big)dx \\ &\quad - \int_0^{\theta_1} e^{-\frac{\rho x}{\beta_{ua}}} K_0\Big(2\sqrt{\tfrac{x}{\beta_{ab}\beta_{ua}}}\Big)dx\Bigg] \\ &= \frac{2e^{-\frac{\theta_3}{\beta_{ub}}}}{\beta_{ab}\beta_{ua}}\Bigg[\sqrt{\tfrac{\beta_{ab}\beta_{ua}\beta_{ub}}{4\rho}} e^{\frac{\beta_{ub}}{2\rho\beta_{ab}\beta_{ua}}} W_{-\frac{1}{2},0}\Big(\tfrac{\beta_{ub}}{\rho\beta_{ab}\beta_{ua}}\Big) \\ &\quad - \frac{\pi\theta_1}{2N}\sum_{j=0}^{N} e^{\frac{\rho\theta_1(\phi_j+1)}{2\beta_{ua}}} K_0\Big(2\sqrt{\tfrac{\theta_1(\phi_j+1)}{2\beta_{ab}\beta_{ua}}}\Big)\sqrt{1-\phi_j^2}\Bigg] \end{aligned} \tag{52}$$

The first integral in the forth equality in (52) is solved using the identity [41, Eq. (6.614.4)]. By substituting (52) into (51), we obtain (33).

Appendix D
Proof of Lemma 5

The outage probability in (36) can be rewritten as

$$P_{out,c}^{\mathrm{T3(b)}} = 1 - I_4(1 - I_5) \tag{53}$$

where $I_5 = \Pr\Big[\gamma_{b,c}^{\mathrm{T3(b)}} < 2^{2R_o} - 1\Big] = 1 - e^{-\frac{\theta_3}{\beta_{bu}}}$, and the probability I_4 is given as follows

$$\begin{aligned} I_4 &= \Pr\Big[\gamma_{u,x}^{\mathrm{T3(b)}} \geq 2^{R_1} - 1,\ \gamma_{u,c}^{\mathrm{T3(b)}} \geq 2^{2R_o} - 1\Big] \\ &= \frac{2e^{-\frac{\theta_3}{\beta_{bu}}}}{\beta_{au}\beta_{ba}}\Bigg[\sqrt{\tfrac{\beta_{au}\beta_{ba}\beta_{bu}}{4\rho}} e^{\frac{\beta_{bu}}{2\rho\beta_{au}\beta_{ba}}} W_{-\frac{1}{2},0}\Big(\tfrac{\beta_{bu}}{\rho\beta_{au}\beta_{ba}}\Big) \\ &\quad - \frac{\pi\theta_2}{2N}\sum_{j=0}^{N} e^{\frac{\rho\theta_2(\phi_j+1)}{2\beta_{ba}}} K_0\Big(2\sqrt{\tfrac{\theta_2(\phi_j+1)}{2\beta_{au}\beta_{ba}}}\Big)\sqrt{1-\phi_j^2}\Bigg] \end{aligned} \tag{54}$$

Equation (54) is obtained following similar steps as those for finding I_3. Substituting for I_4 and I_5 into (53) gives (37).

Appendix E
Proof of Lemma 6

Substituting (11) into (40), we get

$$P_{out,x}^{\mathrm{T3(a)}} = \Pr\left[\left|h_{ub}\right|^2 < (\rho\left|h_{ab}\right|^2\left|h_{ua}\right|^2 + \theta_3)\right]$$
$$= \int_0^\infty (1 - e^{-\frac{\rho x+\theta_3}{\beta_{ub}}}) f_{\left|h_{ab}\right|^2\left|h_{ua}\right|^2}(x)dx$$
$$= 1 - \frac{2e^{-\frac{\theta_3}{\beta_{ub}}}}{\beta_{ab}\beta_{ua}} \int_0^\infty e^{-\frac{\rho x}{\beta_{ub}}} K_0\left(\sqrt{\frac{4x}{\beta_{ab}\beta_{ua}}}\right)dx. \quad (55)$$

Solving the last integral using [41, Eq. (6.614.4)] gives (41).

REFERENCES

[1] M. Vaezi, A. Azari, S. R. Khosravirad, M. Shirvanimoghaddam, M. M. Azari, D. Chasaki, and P. Popovski, "Cellular, wide-area, and non-terrestrial IoT: A survey on 5G advances and the road toward 6G," *IEEE Commun. Surveys Tuts.*, vol. 24, no. 2, pp. 1117–1174, 2022.

[2] F. Guo, F. R. Yu, H. Zhang, X. Li, H. Ji, and V. C. M. Leung, "Enabling massive IoT toward 6G: A comprehensive survey," *IEEE Internet Things J.*, vol. 8, no. 15, pp. 11 891–11 915, 2021.

[3] W. Yang, M. Wang, J. Zhang, J. Zou, M. Hua, T. Xia, and X. You, "Narrowband wireless access for low-power massive internet of things: A bandwidth perspective," *IEEE Wireless Commun.*, vol. 24, no. 3, pp. 138–145, 2017.

[4] N. Varsier, L.-A. Dufrène, M. Dumay, Q. Lampin, and J. Schwoerer, "A 5G new radio for balanced and mixed IoT use cases: Challenges and key enablers in FR1 band," *IEEE Commun. Mag.*, vol. 59, no. 4, pp. 82–87, 2021.

[5] 3GPP, TR-22.840, "Study on ambient power-enabled Internet of things," Tech. Rep., 2023.

[6] 3GPP, TR-38.848, "Study on ambient IoT (Internet of things) in RAN," Tech. Rep., 2023.

[7] C. Xu, L. Yang, and P. Zhang, "Practical backscatter communication systems for battery-free Internet of things: A tutorial and survey of recent research," *IEEE Signal Process. Mag.*, vol. 35, no. 5, pp. 16–27, Sep. 2018.

[8] S. Naser, L. Bariah, S. Muhaidat, and E. Basar, "Zero-energy devices empowered 6G networks: Opportunities, key technologies, and challenges," *IEEE Internet Things Mag.*, vol. 6, no. 3, pp. 44–50, 2023.

[9] N. V. Huynh, D. T. Hoang, X. Lu, D. Niyato, P. Wang, and D. I. Kim, "Ambient backscatter communications: A contemporary survey," *IEEE Commun. Surveys Tuts.*, vol. 20, no. 4, pp. 2889–2922, 4th Quart. 2018.

[10] T. Jiang, Y. Zhang, W. Ma, M. Peng, Y. Peng, M. Feng, and G. Liu, "Backscatter communication meets practical battery-free internet of things: A survey and outlook," *IEEE Commun. Surveys Tuts.*, vol. 25, no. 3, pp. 2021–2051, 2023.

[11] A. Al-Nahari, R. Jäntti, D. Mishra, and J. Hämäläinen, "Massive MIMO beamforming in monostatic backscatter multi-tag networks," *IEEE Commun. Lett.*, vol. 25, no. 4, pp. 1323–1327, 2021.

[12] R. Duan, X. Wang, H. Yigitler, M. U. Sheikh, R. Jantti, and Z. Han, "Ambient backscatter communications for future ultra-low-power machine type communications: Challenges, solutions, opportunities, and future research trends," *IEEE Commun. Mag.*, vol. 58, no. 2, pp. 42–47, 2020.

[13] M. M. Butt, N. R. Mangalvedhe, N. K. Pratas, J. Harrebek, J. Kimionis, M. Tayyab, O.-E. Barbu, R. Ratasuk, and B. Vejlgaard, "Ambient IoT: A missing link in 3GPP IoT devices landscape," *IEEE Internet Things Mag.*, vol. 7, no. 2, pp. 85–92, 2024.

[14] S. A. Ahson and M. Ilyas, *RFID handbook: applications, technology, security, and privacy*. CRC press, 2017.

[15] A. Al-Nahari, R. Jäntti, R. Duan, D. Mishra, and H. Yiğitler, "Multi-bounce effect in multi-tag monostatic backscatter communications," *IEEE Wireless Commun. Lett.*, vol. 11, no. 1, pp. 43–47, 2022.

[16] M. U. Sheikh, F. Jameel, H. Yiğitler, X. Wang, and R. Jäntti, "Monostatic backscatter communication in urban microcellular environment using cellular networks," in *2020 IEEE Wireless Commun. Net. Conf. (WCNC)*, 2020, pp. 1–6.

[17] C. He, S. Chen, H. Luan, X. Chen, and Z. J. Wang, "Monostatic MIMO backscatter communications," *IEEE J. Sel. Areas Commun.*, vol. 38, no. 8, pp. 1896–1909, 2020.

[18] J. Kimionis, A. Bletsas, and J. Sahalos, "Increased range bistatic scatter radio," *IEEE Trans. Commun.*, vol. 62, no. 3, pp. 1091–1104, Mar. 2014.

[19] V. Liu, A. Parks, V. Talla, S. Gollakota, D. Wetherall, and J. R. Smith, "Ambient backscatter: wireless communication out of thin air." New York, NY, USA: Association for Computing Machinery, 2013. [Online]. Available: https://doi.org/10.1145/2486001.2486015

[20] W. Zhao, G. Wang, S. Atapattu, C. Tellambura, and H. Guan, "Outage analysis of ambient backscatter communication systems," *IEEE Commun. Lett.*, vol. 22, no. 8, pp. 1736–1739, 2018.

[21] W. Zhao, G. Wang, R. Fan, L.-S. Fan, and S. Atapattu, "Ambient backscatter communication systems: Capacity and outage performance analysis," *IEEE Access*, vol. 6, pp. 22 695–22 704, 2018.

[22] Y. Ye, L. Shi, X. Chu, and G. Lu, "On the outage performance of ambient backscatter communications," *IEEE Internet Things J.*, vol. 7, no. 8, pp. 7265–7278, 2020.

[23] R. Long, Y.-C. Liang, H. Guo, G. Yang, and R. Zhang, "Symbiotic radio: A new communication paradigm for passive Internet of Things," *IEEE Internet Things J.*, vol. 7, no. 2, pp. 1350–1363, 2020.

[24] Y.-C. Liang, Q. Zhang, E. G. Larsson, and G. Y. Li, "Symbiotic radio: Cognitive backscattering communications for future wireless networks," *IEEE Trans. Cogn. Commun. Netw.*, vol. 6, no. 4, pp. 1242–1255, 2020.

[25] A. Al-nahari, R. Jäntti, G. Zheng, D. Mishra, and M. Nie, "Ergodic secrecy rate analysis and optimal power allocation for symbiotic radio networks," *IEEE Access*, vol. 11, pp. 82 327–82 337, 2023.

[26] M. Nie, D. Mishra, A. Al-nahari, J. Yuan, and R. Jäntti, "QoS awareness transmit beamforming for secure backscattering in symbiotic radio networks," *IEEE Systems Journal*, vol. 18, no. 2, pp. 1356–1367, 2024.

[27] H. Ding, D. B. da Costa, and J. Ge, "Outage analysis for cooperative ambient backscatter systems," *IEEE Wireless Commun. Lett.*, vol. 9, no. 5, pp. 601–605, 2020.

[28] H. Guo, Y.-C. Liang, R. Long, and Q. Zhang, "Cooperative ambient backscatter system: A symbiotic radio paradigm for passive IoT," *IEEE Wireless Commun. Lett.*, vol. 8, no. 4, pp. 1191–1194, 2019.

[29] D. Zhang and Q. Zhu, "Outage analysis for multi-BD symbiotic radio system," *IET Communications*, vol. 16, no. 19, pp. 2301–2308, 2022.

[30] H. Ding, M.-S. Alouini, K. Xin, H. Li, and S. Xu, "Symbiotic ambient backscatter systems: Outage behavior and ergodic capacity," *IEEE Internet Things J.*, vol. 9, no. 23, pp. 23 670–23 690, 2022.

[31] Y. Tuo and C. Zhang, "Outage analysis of parasitic ambient backscatter communication in decode-and-forward relay networks with SWIPT," *Sensors*, vol. 20, no. 5, 2020.

[32] X. Song, D. Han, L. Shi, H. Sun, and R. Q. Hu, "Relay assisted cooperative ambient backscatter communication with hybrid long-short packets," *IEEE Trans. Veh. Technol.*, pp. 1–14, 2024.

[33] P. Yang, W. Kuang, and S. Wang, "Relay selection for dual-hop cooperative ambient backscatter communication systems," *Sensors*, vol. 23, no. 13, 2023.

[34] J. Liao, K. Ruttik, R. Jäntti, and D.-T. Phan-Huy, "Demo: UE assisted ambient IoT in LTE downlink, in real-time and open source," in *Proceedings of the 21st Annual International Conference on Mobile Systems, Applications and Services*, ser. MobiSys '23, New York, NY, USA, 2023, p. 588–589.

[35] J. Liao, X. Wang, K. Ruttik, R. Jäntti, and D.-T. Phan-Huy, "In-band ambient FSK backscatter communications leveraging LTE cell-specific reference signals," *IEEE J. Radio Freq. Identif.*, vol. 7, pp. 267–277, 2023.

[36] A. J. S. Boaventura and N. B. Carvalho, "The design of a high-performance multisine RFID reader," *IEEE Trans. Microw. Theory Techn.*, vol. 65, no. 9, pp. 3389–3400, 2017.

[37] D. Mishra and E. G. Larsson, "Optimal channel estimation for reciprocity-based backscattering with a full-duplex MIMO reader," *IEEE Trans. Signal Process.*, vol. 67, no. 6, pp. 1662–1677, 2019.

[38] N.-C. Kuo and A. M. Niknejad, "Single-antenna FDD reader design and communication to a commercial UHF RFID tag," *IEEE Microw. Wireless Componen. Lett.*, vol. 28, no. 7, pp. 630–632, 2018.

[39] J. Laneman, D. Tse, and G. Wornell, "Cooperative diversity in wireless networks: Efficient protocols and outage behavior," *IEEE Trans. on Inf. Theory*, vol. 50, no. 12, pp. 3062–3080, 2004.

[40] A. Al-nahari, I. Krikidis, A. Ibrahim, M. Dessouky, and F. Abd El-Samie, "Relaying techniques for enhancing the physical layer secrecy in cooperative networks with multiple eavesdroppers," *Trans. Emerging Telecommun. Technol.*, vol. 25, no. 4, pp. 445–460, 2014.

[41] I. S. Gradshteyn and I. M. Ryzhik, *Table of Integrals, Series, and Products*, 7th ed. New York, NY, USA: Elsevier, 2007.

[42] Y. Zhang, F. Gao, L. Fan, X. Lei, and G. K. Karagiannidis, "Secure communications for multi-tag backscatter systems," *IEEE Wireless Commun. Lett.*, vol. 8, no. 4, pp. 1146–1149, 2019.

[43] E. Biglieri, R. Calderbank, A. Constantinides, A. Goldsmith, A. Paulraj, and H. V. Poor, *MIMO Wireless Communications*. USA: Cambridge University Press, 2007.

[44] K. J. R. Liu, A. K. Sadek, W. Su, and A. Kwasinski, *Cooperative Communications and Networking*. Cambridge University Press, 2008.

[45] F. Olver, D. W. Lozier, R. Boisvert, and C. Clark., *NIST Handbook of Mathematical Functions*. Cambridge Univ. Press, 2010.

[46] W. R. Inc., "Mathematica, Version 13.3," champaign, IL, 2023. [Online]. Available: https://www.wolfram.com/mathematica

[47] C. Hoymann, D. Larsson, H. Koorapaty, and J.-F. Cheng, "A lean carrier for LTE," *IEEE Commun. Mag.*, vol. 51, no. 2, pp. 74–80, 2013.

[48] X. Li, Y. Zheng, W. U. Khan, M. Zeng, D. Li, G. K. Ragesh, and L. Li, "Physical layer security of cognitive ambient backscatter communications for green internet-of-things," *IEEE Trans. Green Commun. Net.*, vol. 5, no. 3, pp. 1066–1076, 2021.

[49] B. Gu, D. Li, Y. Liu, and Y. Xu, "Exploiting constructive interference for backscatter communication systems," *IEEE Trans. Commun.*, vol. 71, no. 7, pp. 4344–4359, 2023.

[50] 3GPP, TR-38.769, "Study on solutions for ambient IoT (Internet of things) NR," Tech. Rep., 2024.

[51] Q. Li, Y. Feng, M. Wen, J. Wen, G. C. Alexandropoulos, E. Basar, and H. Vincent Poor, "Cooperative backscatter communications with reconfigurable intelligent surfaces: An APSK approach," *IEEE Trans. Wireless Commun.*, vol. 23, no. 11, pp. 16 218–16 233, 2024.

[52] B. Gu, D. Li, H. Ding, G. Wang, and C. Tellambura, "Breaking the interference and fading gridlock in backscatter communications: State-of-the-art, design challenges, and future directions," *IEEE Commun. Surveys Tuts.*, vol. 27, no. 2, pp. 870–911, 2025.

[53] S. Basharat, S. A. Hassan, A. Mahmood, Z. Ding, and M. Gidlund, "Reconfigurable intelligent surface-assisted backscatter communication: A new frontier for enabling 6G IoT networks," *IEEE Wireless Commun.*, vol. 29, no. 6, pp. 96–103, 2022.

Azzam Al-nahari received the B.Sc. degree in electronics and communications engineering from the University of Technology, Iraq, and the M.Sc. and Ph.D. degrees in electrical communications from the Faculty of Electronic Engineering, Menoufia University, Egypt, in 2008 and 2011, respectively. Since 2011, he was an Assistant Professor with the Department of Electrical Engineering, Ibb University, Yemen, and became an Associate Professor, in 2017. In 2012, he held a postdoctoral position with the Department of Electrical and Information Technology, Lund University, Sweden. He also held a postdoctoral position with University at Buffalo, Buffalo, NY, USA, in 2014. Since July 2019, he has been a Visiting Scholar with the Department of Information and Communications Engineering, Aalto University, Espoo, Finland. His current research interests include backscatter communications, massive MIMO systems, physical layer security, cognitive radio networks, machine learning and signal processing for wireless communications.

Riku Jäntti (Senior Member, IEEE) received the M.Sc. degree (with distinction) in electrical engineering and the D.Sc. degree (with distinction) in automation and systems technology from the Helsinki University of Technology (TKK) in 1997 and 2001, respectively. He is currently a Full Professor of communications engineering at the Department of Information and Communications Engineering, Aalto University, Finland. Prior to joining Aalto (formerly known as TKK) in August 2006, he was a Professor Pro Tem with the Department of Computer Science, University of Vaasa. His research interests include machine type communications, disaggregated radio access networks, backscatter communications, quantum communications, and radio frequency inference. He is a member of the Editorial Board of IEEE TRANSACTIONS ON COGNITIVE COMMUNICATIONS AND NETWORKING. He has been a IEEE VTS Distinguished Lecturer (Class 2016).

Deepak Mishra (Senior Member, IEEE) received the Ph.D. degree in electrical engineering from Indian Institute of Technology (IIT), Delhi, India, in 2017. He is currently a Senior Lecturer with the School of Electrical Engineering and Telecommunications, University of New South Wales (UNSW) Sydney, Australia, where he joined as a Senior Research Associate, in August 2019. Before that, he was a Postdoctoral Researcher with Linköping University, Sweden, from August 2017 to July 2019. He has also been a Visiting Researcher with Northeastern University, USA, the University of Rochester, USA, Huawei Technologies, France, Southwest Jiaotong University, China, and Queen's University of Belfast, U.K. His current research interests include energy harvesting cooperative communication networks, MIMO, backscattering, physical layer security, and signal processing and energy optimization schemes for the uninterrupted operation of wireless networks. He was a recipient of the IBM PhD Fellowship Award, in 2016, the Raman Charpak Fellowship Award, in 2017, the Endeavour Research Fellowship Award, in 2018, and the Australian Research Council Discovery Early Career Researcher Award, in 2022. He is an Associate Editor of IEEE Transactions on Communications, IEEE Transactions on Green Communications and Networking, IEEE Transactions on Intelligent Vehicles, IEEE Wireless Communications Letters, and IEEE Access.

Yi Zhou (Member, IEEE) received her Ph.D. degree from University of Sydney, Australia, in 2020. Since 2021, she has been with School of Information Science and Technology, Southwest Jiaotong University, China. Her research interests include physical layer security, UAV communications, and 5G related communications. She was a recipient of the Postgraduate Scholarship and the Norman I. Price Scholarship from the Center of Excellence in Telecommunications, School of Electrical and Information Engineering, University of Sydney. She was a recipient of Marie Skłodowska Curie Postdoctoral Fellowship.